EVOLVING SCATTERING PICTURES IN ^{4}He+^{40}Ca SYSTEM AT E=1…25 MeV/NUCLEON

V.Yu. Korda[1], L.P. Korda[2], V.F. Klepikov[1]
[1]Institute of Electrophysics and Radiation Technologies, National Academy of Sciences, Kharkiv, Ukraine;
[2]NSC "Kharkiv Institute of Physics and Technology", Kharkiv, Ukraine

Scattering pictures in ^{4}He+^{40}Ca system, from rainbow scattering to anomalous large angle scattering (ALAS) and down to near Coulomb barrier scattering (NCBS), are systematically explained using the scattering matrix approach in which the nuclear absorption and refraction phases are smooth monotonic functions of angular momentum and the quantum deflection function is of the rainbow-like form and the artificial intelligence evolutionary computations technique.

PACS: 24.10.Ht, 25.55.−e, 25.60.Bx

1. SCATTERING PICTURES OBSERVED IN ^{4}He+^{40}Ca SYSTEM AT E=1…25 MeV/NUCLEON

The nuclear-nuclear interaction at energies of 1…25 MeV/nucleon is characterized by a variety of scattering patterns. For example [1–12] (Fig. 1), in the measured differential cross section (normalized to the Rutherford cross section) of elastic scattering of α-particles by ^{40}Ca nuclei σ/σ_R at energies of about 20 MeV/nucleon (82 MeV on Fig. 1), a nuclear rainbow pattern is observed with a characteristic broad maximum and a subsequent regular exponential decrease in the cross section at large scattering angles θ. With decreasing energy, a nuclear pre-rainbow pattern appears (61 MeV on Fig. 1) with various interference structures, for example, Airy structures of different orders (minima of the Airy function are marked as A1,2,3 on Fig. 1) and a violation of the regular exponential decrease in the cross section at large angles. With further energy reduction, a pattern of ano-malous large-angle scattering (ALAS) is observed (22…49.5 MeV on Fig. 1) with an unusual increase of orders of magnitude in the oscillating cross section in the large-angle region. Further energy reduction leads to a sequential transformation of this pattern into a scattering pattern near the Coulomb barrier (NCBS) with suppression of cross section oscillations and an increase in the influence of the Coulomb interaction (4.5…18 MeV on Fig. 1).

Thus far, to our knowledge, neither the smoothly varying global optical potential, nor the single potential family has been found to describe all the variety of scattering pictures observed in the ^{4}He-^{40}Ca elastic scattering at E<25 MeV/nucleon.

Using the evolutionary S-matrix approach developed by us [13,14], we have for the first time obtained a unified consistent systematic description of all the mentioned scattering patterns [15,16].

2. EVOLUTIONARY MODEL-INDEPENDENT SCATTERING MATRIX APPROACH

In our approach, the scattering matrix describing the ^{4}He-^{40}Ca elastic scattering has the form

$$S(l) = S_N(l)\exp[2i\sigma_C(l)], \qquad (1)$$

where

$$S_N(l) = \eta(l)\exp[2i\sigma_r(l)], \qquad (2)$$

is the nuclear part, $\sigma_C(l)$ is the Coulomb scattering phase taken to be the quasiclassical phase of point-charge scattering by a uniformly charged sphere with the radius R_C=1.3×40$^{1/3}$ at above-Coulomb-barrier energies and the ordinary Coulomb phase for scattering of two point charges at lower energies,

$$\eta(l) = \exp[-2\sigma_a(l)], \qquad (3)$$

is the scattering matrix modulus, $\delta_r(l)$ is the nuclear refraction phase (real part of the nuclear phase), and $\delta_a(l)$ is the nuclear absorption phase (imaginary part of the nuclear phase). Calculations are performed usi

ng the expansion of the scattering amplitude into a series of Legendre polynomials. The elastic scattering differential cross section equals the squared modulus of this amplitude. The quality of fitting the calculated differential cross section to the experimentally measured one is estimated using the standard χ^2 magnitude per datum. The experimental errors are assumed to be equally weighted (10% error bars).

More detailed analysis of complicated structures inherent in the elastic scattering cross sections under discussion can be performed with the use of the nearside-farside decomposition. To detect the Airy structures, we use both the farside component and the farside component calculated without absorption in the scattering matrix [$\eta(l)$=1 for all l].

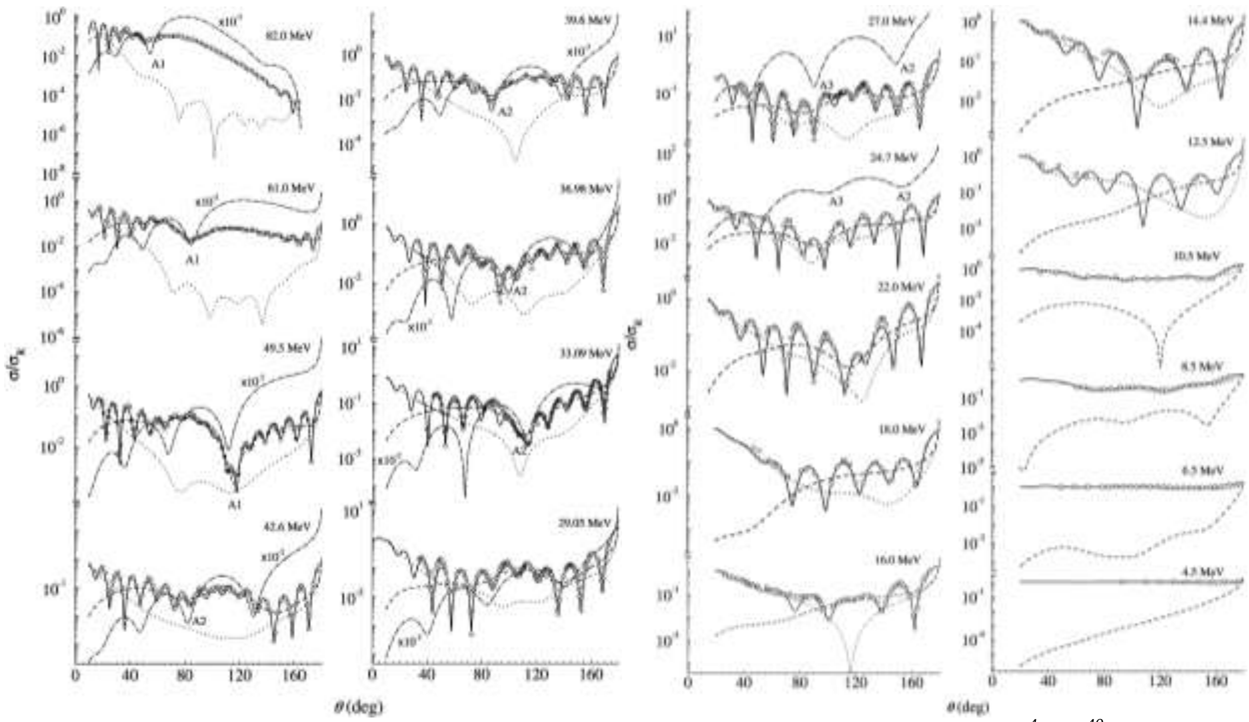

Fig. 1. Elastic scattering differential cross sections (ratio to Rutherford) for the system $^4He+^{40}Ca$ *at* E=4.5…82.0 *MeV (solid curves), their farside (dashed curves) and nearside (dotted curves) components, and farside cross-section components calculated without absorption in the scattering matrix (dash-dotted curves). A1, A2 and A3 denote the Airy minima of first, second and third orders. The data are from Refs.* [1–12]

Our evolutionary model-independent S-matrix approach [14–16] operates on a population of N individuals. Each individual is an S matrix presented as a pair of real-valued $l_{\max}$ dimensional vectors $[\delta_a(l),\delta_r(l)]$, l = 0,1,...,$l_{\max}-1$. Fitness of each individual reflects the quality of data fitting provided by the individual's S matrix. Using the mutation operation, the algorithm evolves the initial population of poorly fitted individuals to the final population of the well-fitted ones. Every iteration, the so-called generation, of our procedure contains the following steps.

(1) Generating the initial population of N individuals. For each individual, vectors $\delta_{a,r}(l)$ are set using a physically justified function:

$$2\delta_i(l) = g_i\, f(l,l_i,d_i),$$

$$f(l,l_i,d_i) = \left[1+\exp\left(\frac{l-l_i}{d_i}\right)\right]^{-1},\ i=a,r. \tag{4}$$

Parameters g_i, l_i , and d_i are positive and are chosen for each individual at random within certain intervals wide enough to obtain substantially different shapes of the phases.

(2) Evaluating fitness of each individual in the population. The fitness function in our approach consists of two parts. The first one is associated with the quality of shapes of $\delta_{a,r}(l)$, and the second one accounts for the quality of fitting of the experimental data. Shapes of $\delta_{a,r}(l)$ must meet the following requirements:

(i) Functions $\delta_{a,r}(l)$ must be descending.

(ii) The first derivatives of $\delta_{a,r}(l)$ must have only one minimum and no maxima.

(iii) The second derivatives of $\delta_{a,r}(l)$ are allowed to have one deepest minimum, one highest maximum, and an arbitrary number of local minima and maxima that do not substantially influence the shapes of phases.

(iv) The third derivative of $\delta_r(l)$ is allowed to have two deepest minima, one highest maximum, and an arbitrary number of local minima and maxima that do not substantially influence the shape of the real nuclear phase.

(v) Logarithmic derivatives of $\delta_{a,r}$ (l) should be descending in the phase tail region. The individual for which at least one of these requirements is violated is excluded from the population.

(3) Letting each individual in the population produce M>>1 offspring. Replication is performed according to the transformation:

$$\log[\delta_i{}'(l)] = \log[\delta_i(l)] + A_i N_i(0,1) D(l,l_{m,i},d_{m,i}),$$
$$i=a,r, \tag{5}$$

where $\delta_i(l)$ and $\delta_i{}'(l)$ are the parent's and the offspring's S-matrix phases, respectively, A_i>0 is the mutation amplitude, $A_i\in[A_{\min},A_{\max}]$, $N_i(0,1)$ denotes a normally distributed one-dimensional random number with mean zero and one standard deviation, $D(l,l_{m,i},d_{m,i})$ is the mutation diffusing function, $l_{m,i}$ stands for the mutation point chosen randomly, $l_{m,i}\in[0,l_{\max}-1]$, and $d_{m,i}$>0 is the value characterizing the diffuseness of the mutation point, $d_{m,i}\in[d_{\min},d_{\max}]$. The mutation diffusing function has the form

$$D(l,l_{m,i},d_{m,i}) = \exp\left[\frac{(l-l_{m,i})^2}{d_{m,i}^2}\right]. \tag{6}$$

During the replication of the parent, the values of mutation amplitude and diffuseness are tuned within he specified intervals as follows:

$$A_i{}' = A_i \exp[L N_i(0,1)],$$

$$d_{m,i}' = d_{m,i}\exp\left[LN_i(0,1)\right], \qquad (7)$$

where A_i and $d_{m,i}$ are the values of mutation amplitude and diffuseness of the parent, while A_i and $d_{m,i}$ are the same values of the offspring, respectively, L is the learning parameter that controls the speed of tuning. The lengths of the intervals $[A_{\min},A_{\max}]$ and $[d_{\min},d_{\max}]$, having large values at the beginning of the procedure, smoothly decrease during the run and acquire small values at the end. This tactic provides for both removal of the features of primary parametrization (4) from the individual's $S(l)$ and fine tuning of details of $S(l)$.

(4) Evaluating fitness values of all offspring. Sort the ffspring in descending order according to their fitness. Select N best offspring to form the new population.

(5) Going to step 3 or stop if the best fitness in the population is sufficiently high (the χ^2 value is small enough).

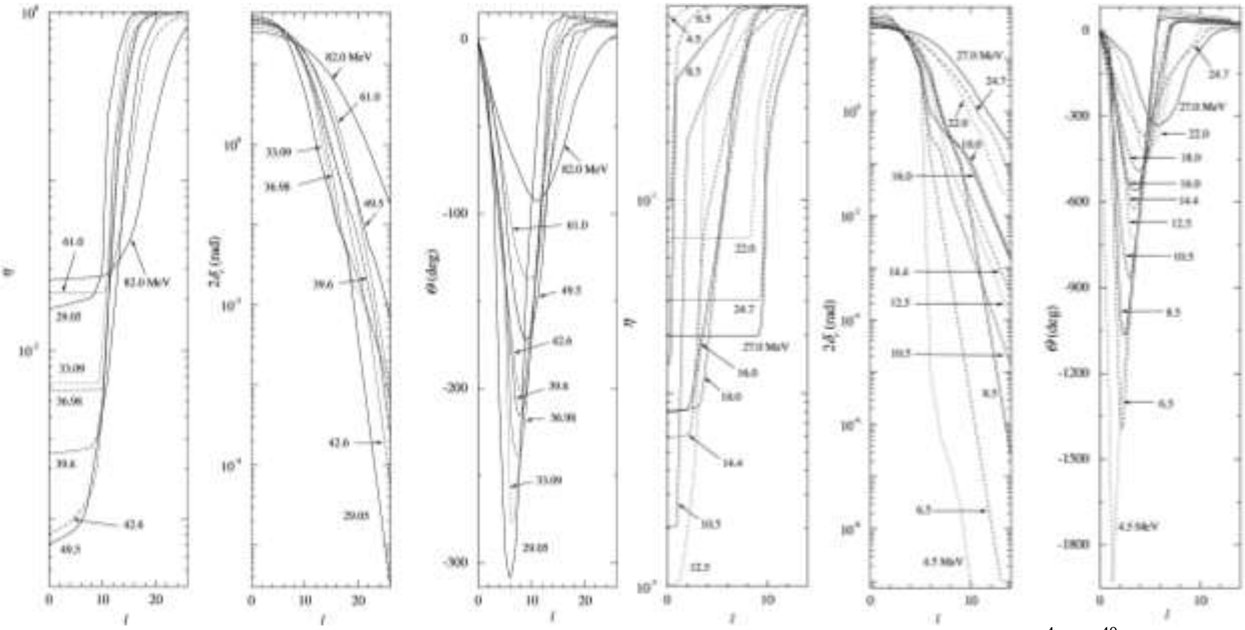

Fig. 2. Scattering matrix moduli $\eta(l)$, nuclear phases $\delta_r(l)$, and deflection functions $\Theta(l)$ for the ^{4}He+^{40}Ca *elastic scattering at E*=4.5…82.0 *MeV*

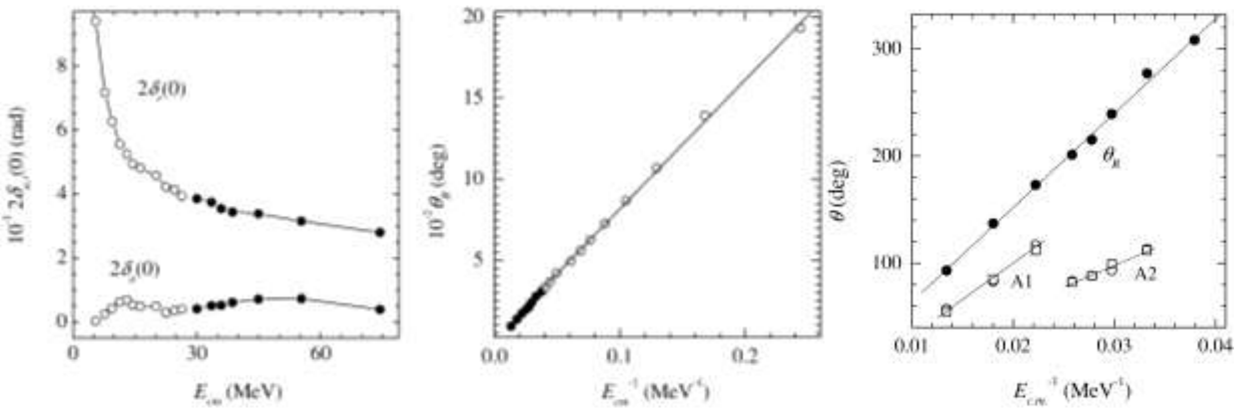

Fig. 3. (a) Evolution with center-of-mass energy of the intensities of nuclear refraction $2\delta_r$ (0) *and nuclear absorption* $2\delta_a(0)$ *for the system* ^{4}He+^{40}Ca. *Solid curves are only to guide the eye. (b) Evolution with reciprocal center-of-mass energy of the nuclear rainbow angle θ_R. Straight line shows results of fitting to the data. Evolution with center-of-mass energy of the angular position of the Airy minima of first A1 and second A2 orders in the measured differential cross sections for the system* ^{4}He+^{40}Ca *(circles) and in the farside cross-section components calculated without absorption in the scattering matrix (squares), Straight lines show results of fitting to the data indicated as circles*

3. RESULTS

In each case under investigation, from nuclear rainbow at sufficiently high energies to ALAS at the lower energies and down to NCBS, the data in the whole angular range considered are correctly described by the differential cross section (see Fig. 1) calculated with the obtained smooth monotonic representations for the scattering matrix modulus and nuclear phase (Fig. 2).

When the energy decreases from 82 to 22 MeV for all analyzed cross sections in the region of large scattering angles, a moderate increase in the dominant farside component of the cross section (see dashed curves on Fig. 1), which is a manifestation of the effects of strong nuclear refraction, and a sharp increase in the nearside component of the cross section (see dotted curves on Fig. 1). The interference of these components, which increases with decreasing energy, causes a transition from the nuclear rainbow pattern to the pattern of anomalous large angle scattering. When the energy decreases from 18 to 12.5 MeV for all analyzed cross sections, a shift of the Fraunhofer crossover point towards large scattering angles is observed. And at energies of 4.5…10.5 MeV, the Fraunhofer crossover point disappears, the nearside component of the cross section dominates for all scattering angles, and the contribution of the farside component is small, which causes the transition from the picture of anomalous large angle scattering to the picture of Coulomb scattering.

In our systematics, the modulus of the scattering matrix η, or the nuclear absorption phase δ_a, and the nuclear refraction phase δ_r are smooth monotonic functions of the angular momentum l, and the quantum deflection function $\Theta(l)=2d[\delta_r(l)+\sigma_C(l)]/dl$ has a form inherent in the rainbow scattering pattern.

The angular positions of the Airy minima A1,2 extracted from the experimental data (circles on Fig. 3 for A1,2) and calculated by us (squares on Fig. 3 for A1,2) obey the law of the inverse collision energy in the center-of-mass system. The nuclear rainbow angle θ_R, which is the minimum of the quantum deflection function (circles on Fig. 3 for θ_R), obeys the same law. The use of such an energy systematics made it possible to get rid of the ambiguities in the description of the experimental data.

With a decrease in the collision energy, the intensity of nuclear refraction [$2\delta_r(l=0)$ on Fig. 3] systematically increases consistently throughout the studied energy range, even in the region of dominance of the Coulomb interaction. That is, we have shown for the first time that the transition to the NCBS pattern occurs in the presence of strong nuclear refraction. With increasing collision energy, the intensity of nuclear absorption [$2\delta_a(l=0)$ on Fig. 3] behaves smoothly: it increases in the region of the NCBS pattern, decreases in the region of the transition to the ALAS pattern, increases in the region of this pattern and decreases in the region of the nuclear rainbow pattern. That is, we have shown for the first time how a change in the intensity of nuclear absorption controls the change in the patterns of nucleus-nucleus scattering.

CONCLUSIONS

Applying the evolutionary model-independent *S*-matrix approach, we have shown that a simultaneous correct description of the whole variety of the scattering pictures observed in the system ^{4}He+^{40}Ca at E=1…21 MeV/nucleon (including pictures of the nuclear rainbow, prerainbow, ALAS, and NCBS) can be achieved in a unified way using *S*-matrix moduli and real nuclear phases, which are smooth and monotonic functions of the angular momentum. The quantum deflection functions have a form characteristic of the nuclear rainbow case and are mostly symmetric in the vicinity of a minimum. The scattering matrix and the quantum deflection function for the system ^{4}He+^{40}Ca at E=4.5…82.0 MeV show smooth physically motivated variations with the projectile energy. The nuclear rainbow angle obeys the law of the reciprocal center-of-mass energy dependence. Systematic description of the ^{4}He-^{40}Ca elastic scattering at E=1…21 MeV/nucleon is achieved in the presence of strong nuclear refraction and is in line with the rainbow interpretation of the data.

The Airy minima of first and second orders have been successfully identified in the differential cross sections of the ^{4}He-^{40}Ca elastic scattering. Their angular positions obey the law of the reciprocal center-of-mass energy dependence, which is in conformity with the rainbow interpretation of the data. The use of this energy systematics has allowed us to get rid of the rainbow-shift ambiguity and, thus, to determine the nuclear part of the scattering matrix more reliably.

REFERENCES

1. H. Löhner, H. Eickhoff, D. Frekers, G. Gaul, K. Poppensieker, R. Santo, A.G. Drentje, and L.W. Put, Investigation of large angle structure in α-scattering from calcium isotopes between E_α=36-61 MeV // *Z. Phys. A*. 1978, v. 286, p. 99-106. https://doi.org/10.1007/BF01434618

2. H.H. Chang, B.W. Ridley, T.H. Braid, T.W. Conlon, E.F. Gibson, and N.S.P. King, Energy dependence of the optical model parameters for α-particles scattered from ^{40}Ca and ^{58}Ni // *Nucl. Phys. A*. 1976, v. 270, p. 413-427. https://doi.org/10.1016/0375-9474(76)90454-1

3. H.H. Chang, B.W. Ridley, T.H. Braid, T.W. Conlon, E.F. Gibson, and N.S.P. King, Energy dependence of the optical model parameters for α-particles scattered from ^{40}Ca and ^{58}Ni // *Nucl. Phys. A*. 1976, v. 270, p. 413-427. https://doi.org/10.1016/0375-9474(76)90454-1

4. H.P. Gubler, U. Kiebele, H.O. Meyer, G.R. Plattner, and I. Sick, Large-angle alpha scattering from ^{40}Ca is not anomalous // *Phys. Lett. B*, 1978, v. 74, p. 202-206. https://doi.org/10.1016/0370-2693(78)90553-1

5. H.P. Gubler, U. Kiebele, H.O. Meyer, G.R. Plattner, and I. Sick, The phenomenological optical potential for α-scattering from nuclei in the Ca region // *Nucl. Phys. A*, 1981, v. 351, p. 29. https://doi.org/10.1016/0375-9474(81)90543-1

6. G. Gaul, H. Lüdecke, R. Santo, H. Schmeing, and R. Stock, Effects of α-particle correlations in elastic α-scattering // *Nucl. Phys. A*. 1969, v. 137, p. 177-192. https://doi.org/10.1016/0375-9474(69)90081-5

7. A. Budzanowski, K. Grotowski, S. Micek, H. Niewodniczański, J. Śliz, A. Strzałkowski, and H. Wojciechowski. Elastic scattering of 24.7 MeV alpha particles // *Phys. Lett.* 1964, 11, 74. https://doi.org/10.1016/0031-9163(64)90265-3

8. M. Makowska-Rzeszutko, A. Dudek, and A. Drzymała, Analysis of the elastic scattering of alpha particles // *Acta Phys. Pol. B*, 1971, v. 2, p. 771-787. https://www.actaphys.uj.edu.pl/fulltext?series=Reg&vol=2&page=771

9. C.P. Robinson, J.P. Aldridge, J. John, and R.H. Davis, Optical-model analysis of alpha-particle scattering by ^{40}Ca from 12 to 18 MeV // *Phys. Rev.* 1968, v. 171, p, 1241.
https://doi.org/10.1103/PhysRev.171.1241

10. J. John, C.P. Robinson, J.P. Aldridge, and R.H. Davis, Shape and compound elastic scattering of α-particles by ^{40}Ca, 5.0 to 12.5 MeV // *Phys. Rev.*, 1969, v 177, p. 1755.
https://doi.org/10.1103/PhysRev.177.1755

11. J.P.F. Sellschop, A. Zucchiatti, L. Mirman, M.Z.I. Gering, and E. Di Salvo, Resonant states in alpha-^{40}Ca elastic scattering // J. Phys. G, 1987, v. 13, p. 1129. https://doi.org/10.1088/0305-4616/13/9/014

12. D. Frekers, R. Santo, and K. Langanke, Identification of quasimolecular resonances in low energy α-^{40}Ca scattering and effects of compound nucleus excitation // *Nucl. Phys. A*. 1983, v. 394, p. 189. https://doi.org/10.1016/0375-9474(83)90169-0

13. V.Yu. Korda, A.S. Molev, L.P. Korda, Evolving model-free scattering matrix via evolutionary algorithm: ^{16}O-^{16}O elastic scattering at 350 MeV // *Phys. Rev. C*. 2005, v. 72, p. 014611.
https://doi.org/10.1103/PhysRevC.72.014611

14. V.Yu. Korda, S.V. Berezovsky, A.S. Molev, V.F. Klepikov, Solving variational problems via evolutionary algorithm // *Int. J. Mod. Phys. C*. 2013, v. 24, №3, p. 1350009.
https://doi.org/10.1142/S0129183113500095

15. V.Yu. Korda, A.S. Molev, L.P. Korda, V.F. Klepikov. Unified model-independent *S*-matrix description of nuclear rainbow, prerainbow, and anomalous large-angle scattering in ^{4}He-^{40}Ca elastic scattering // *Phys. Rev. C*. 2015, v. 91, p. 024619.
https://doi.org/10.1103/PhysRevC.91.024619

16. V.Yu. Korda, A.S. Molev, L.P. Korda, V.F. Klepikov. Systematic model-independent *S*-matrix analysis of 4He-40Ca elastic scattering in going from anomalous large-angle scattering to near-Coulomb-barrier scattering // *Phys. Rev. C*. 2018, v. 97, p. 034606.
https://doi.org/10.1103/PhysRevC.97.034606